Article

Electrochemical Reduction of CO at Functionalized Au Electrodes

Yuxin Fang, and John C. Flake

J. Am. Chem. Soc., **Just Accepted Manuscript** • DOI: 10.1021/jacs.6b11023 • Publication Date (Web): 09 Feb 2017

Electrochemical Reduction of CO_2 at Functionalized Au Electrodes

Yuxin Fang, John C. Flake*

Gordon and Mary Cain Department of Chemical Engineering, Louisiana State University, Baton Rouge, Louisiana 70803

ABSTRACT

Electrochemical reduction of CO_2 provides an opportunity to store renewable energy as fuels with much greater energy densities than batteries. Product selectivity of the reduction reaction is known to be a function of the electrolyte and electrode; however, electrodes modified with functional ligands may offer new methods to control selectivity. Here, we report the electrochemical reduction of CO_2 at functionalized Au surfaces with thiol-tethered ligands including: 2-mercaptopropionic acid, 4-pyridinylethanemercaptan and cysteamine. Remarkably, Au electrodes modified with 4-pyridinylethanemercaptan show a 2-fold increase in Faradaic efficiency and 3-fold increase in formate production relative to Au foil. Conversely, electrodes with 2-mercaptopropionic acid ligands show nearly 100% Faradaic efficiency toward the hydrogen evolution reaction; while cystemine-modified electrodes showed 2-fold increase in both CO and H_2 production. We propose a proton-induced desorption mechanism associated with pKa of the functionalized ligand as responsible for the dramatic selectivity changes.

INTRODUCTION

Fuels made via the electrochemical reduction of CO_2 could allow renewable energy storage with several significant advantages over batteries. The specific energy of fuels such as methanol is at least an order of magnitude greater than the best Li-ion batteries on a volumetric basis; further, other fuels (jet fuel, diesel) used in heavy transportation may be synthesized from electrolytically-generated alcohols. There are also inherent advantages to storing and transporting energy as liquid fuels relative to batteries such as: no self-discharging and relatively low storage costs. Further, it may be possible to operate the entire system in carbon neutral process if atmospheric CO_2 is used as the carbon source.[1]

While the electrochemical reduction of CO_2 has been investigated for over a century, the field was reenergized in 1987 by Hori's work showing Cu electrodes were capable of producing significant amounts of methane and ethylene.[2] Since that time, there have been a number of studies aimed at understanding and improving the selectivity and efficiency of CO_2 reduction reactions.

Metals have been thoroughly investigated as heterogeneous electrocatalysts in various forms ranging from polycrystalline foils to nanoparticles.[3-6] Previous works have shown that Au[3, 7] and Ag[3] foil electrodes primarily produce CO (with 81~93% and 61~90% Faradaic efficiencies ~5 $mAcm^{-2}$ in 0.5M $KHCO_3$, respectively). As mentioned, Cu[2, 8] electrodes produce hydrocarbons with reasonable Faradaic efficiencies (e.g. CH_4: 29.4%; C_2H_4: 30.1% at 5 mA/cm^{-2} in 0.1M $KHCO_3$) but suffer from relatively high overpotential requirements and electrode fouling. Sn electrodes have a relatively high overpotential for the Hydrogen Evolution Reaction (HER) and yield formate as primary product until the formation of SnO_2 deactivates the catalyst.[9] Many consider formate a "dead end" [10] ; that is, no further C-O bond cleavage in CO_2 or hydrogenation occurs; however, it is important to note that formate is a valuable chemical feedstock and fuel.[11] Other metals such as Pt, Ni, Fe, etc. favor the HER at the potentials required for CO_2 reduction and do not produce any appreciable hydrocarbons.[12]

While Cu electrodes remain the most attractive in terms of hydrocarbon production, the potential to hydrogenate CO intermediates and produce other high-value products such as alcohols appears to be limited with conventional electrodes.[13] There are several potential pathways to mitigate the "scaling relations"[13] that limit CO hydrogenation including the use of nanoscale electrodes (exposing atomically precise sites [5,14]), alloys (shifting the d-band center energy level[15,16-17]), surface ligands (forming hydrogen-bond like interactions for intermediates [18]) to stabilize the adsorption of key intermediates (COOH* or CO*) and/or electrode mediators (i.e. those capable of capturing CO_2 [19]).

It is important to note that nature uses all of the aforementioned tools to selectively convert CO_2 to a wonderful variety of products.[20-21] Likewise, there have been some studies showing electrolyte additives such as pyridine or the use of molecular catalysts like pterins lead to the formation of alcohols or other higher value hydrocarbons.[22] Bocarsly et al. showed Faradaic efficiencies up to 30% for CH_3OH at 40 $\mu A/cm^2$ on Pd/Pt using 10mM pyridine additives to the electrolyte.[23] The pyridinium ($pyrH^+$) was proposed as the active homogenous catalysts until later studies suggested that the pyridinium radical ($pyrH^*$) functioned as one-electron charge-transfer mediator for the production of methanol at the electrode surface.[24-25] Further pyridine substituted groups yielded up to 30% Faradaic efficiency to CH_3OH production; however, these results were generated at relatively low current densities (~50 $\mu A/cm^2$). [26] Likewise Dyer et al. studied the use of pterins, namely mercaptopteridine (PTE) as molecular catalysts in 0.1M KCl at glassy carbon electrodes that yielded 10~24% CH_3OH at 100 $\mu A/cm^2$ which was similarly attributed to the electron transfer ability of pterin.[22]

In this work we focus on CO_2 reduction and hydrogenation via monolayers of thiol-tethered functional ligands on Au electrodes. Au was chosen as the substrate since it is noble and forms strong S-Au covalent bonds[27]. Three ligands: 2-mercaptopropionic acid (MPA), 4-pyridylethylmercaptan (4-PEM) and cystemine (CYS) were selected as the functional ligands because of their pKa range from low to high (3.7, 5.2, 9.25). The gas and liquid products at the

surface modified electrodes are analyzed as well as the stability of the ligand-modified modified surfaces.

Results and Discussion

Product Analysis

Figure 1 shows the potential dependent product distribution (expressed in Faradaic efficiency for selectivity and partial current density for yield of each compound) from CO_2 reduction on functionalized-Au and untreated Au surfaces. The primary products including formate, CO and H_2 were characterized by NMR and GC analysis. Their potential dependent yield behavior and Faradaic efficiencies are discussed in the following sections.

Relative to untreated Au foil, MPA modified Au electrodes produced hydrogen as a primary product (Faradaic efficiency near 100%) in the low overpotential range (>-0.8V vs. RHE) while CO evolution was suppressed. The greatest observed Faradaic efficiency for CO evolution is less than 20% which is roughly half of that on untreated Au. Likewise, the formate production is reduced by approximately half when MPA is tethered to the electrode. The potential range investigated using MPA modified Au was limited to less than -0.94 V vs. RHE, due to desorption of surface ligands at high overpotentials which is discussed later.

Remarkably, the 4-PEM modified electrodes produced approximately 3 times more formate (-4.1 mA/cm^2) relative to the optimal observed on Au foil (-1.37 mA/cm^2). In terms of the Faradaic efficiency for the reduction to formate, a maxima of 21% with Au/4-PEM electrode (at -1.00V vs. RHE) was achieved compared with 11% on Au surfaces (at -1.01V vs. RHE). On the other hand, the CO partial current was suppressed on the same electrode by at least half relative to Au over the entire potential range of interest. It is interesting to note that the 4-PEM modified Au shows selectivity toward the HER at low potentials (-0.5 to -0.7V vs. RHE), then CO_2 reduction increases in the potential range from -0.7 to -1.1V vs. RHE. Electrolysis in N_2 saturated electrolyte experiments were employed to rule out the possibility of thiolate decomposition into formate.

As for the CYS-functionalized Au electrode, formate production was suppressed relative to Au within the entire potential range of interest. Although the selectivities of CO and H_2 were similar to Au foil, the electrode was significantly more active (i.e. the partial current density j_{CO} and j_{H2} were increased by more than 2 fold).

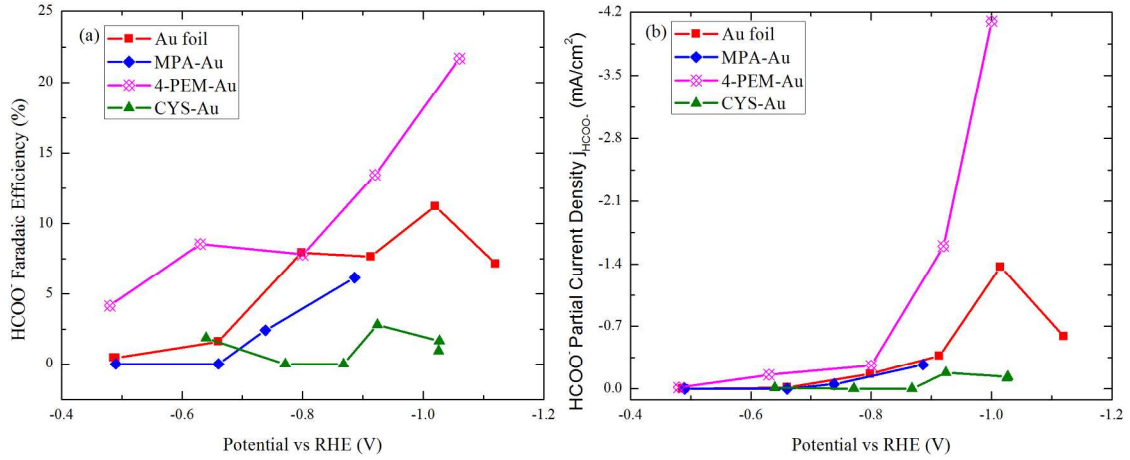

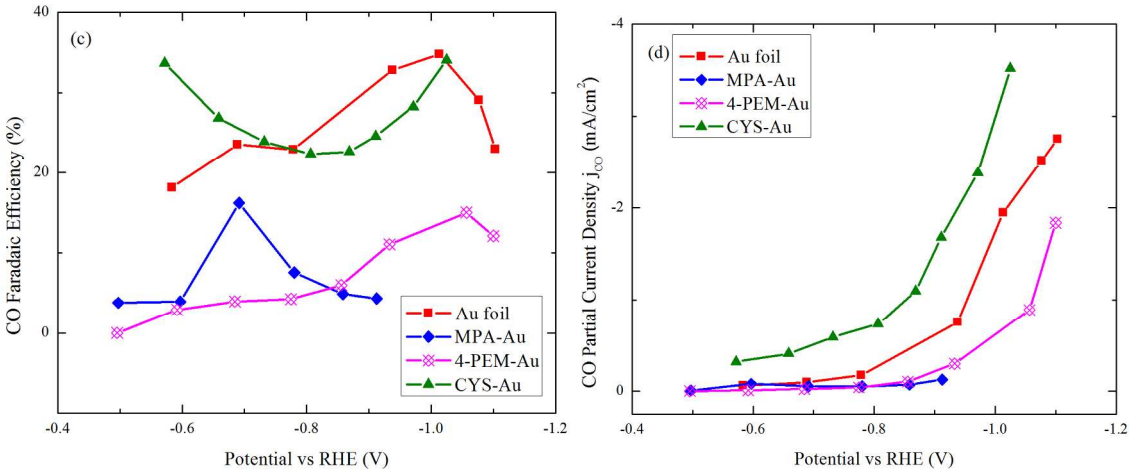

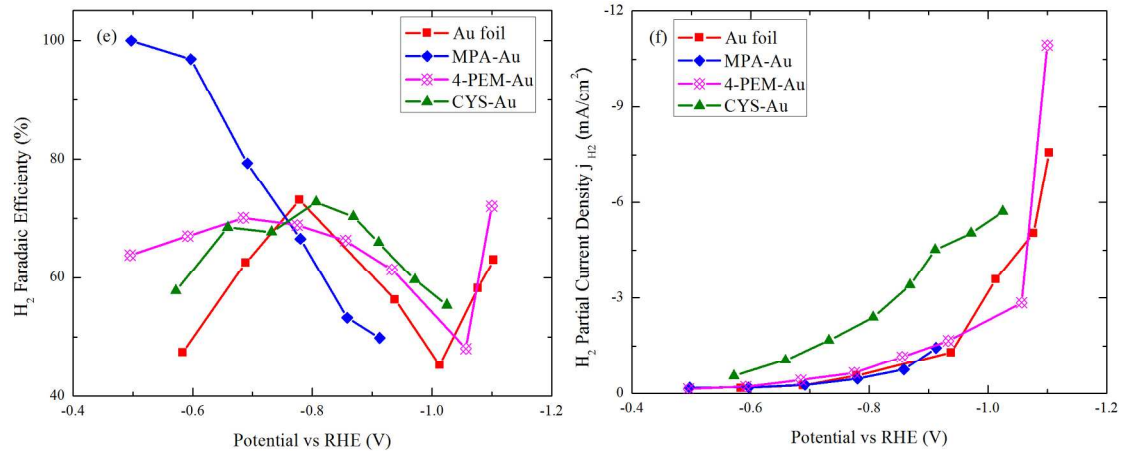

Figure 1.: Comparison of partial current density and Faradaic efficiency (FE) for thiolate ligand on polycrystalline Au and pure polycrystalline Au (a) FE of Formate formation; (±2.5% at 95% Confidence Level (CL) (b) FE of CO formation; (±6.2% at 95% CL) (c) FE of H_2 formation (± 25% at 95% CL); (d) Partial current density of formate formation; (e) Partial current density of CO formation (e) Partial current density of H_2 formation.

Table 1 summarizes the onset potentials for HER and CO_2 reduction on (functionalized) Au substrates. On the MPA functionalized Au, onset potentials for HER and CO_2 reduction were both shifted anodically (by +10 mV and +100 mV respectively). With the 4-PEM functionalized Au electrode, the HER onset potential was shifted cathodically (-50 mV) and the onset potential of CO_2 reduction was shifted anodically (+30mV). On the CYS functionalized Au, both onset potentials were shifted anodically (+90 mV and +70 mV, respectively). The enhancement in Faradaic selectivity toward HER on MPA and 4-PEM functionalized Au may be associated with the decreased onset potential differences (E_{HER}^0- E_{CO2}^0) following ligand modification. The correlation between HER selectivity change (S_1/S_2) and onset potential difference may be expressed in a Butler-Volmer relationship. For example, Equation 1a shows yields in terms of the reactant concentration C_H, C_C, transfer coefficient α, normalized Faraday's constant f and time t (see SI Equation S1 to S5).[28] Assuming similar concentrations of H^+ and CO_2, the Equation 1a can be simplified into Equation 2; thus, the decrease in the difference of onset potentials results in increased HER selectivity. On CYS functionalized Au, the onset potential shifts anodically for both reactions so the product selectivity remains roughly equivalent to the untreated Au electrode.

Table 1: Summarizes the onset potential of HER and CO_2 reduction and their difference on (functionalized)Au surface

Surface	HER (V vs. RHE)	CO_2 Reduction (V vs. RHE)	V_{HER}-V_{CO2RR} (mV)
Au	-0.30	-0.42	120
MPA-Au	-0.29	-0.32	30
4-PEM-Au	-0.35	-0.39	40
CYS-Au	-0.21	-0.35	140

$$\frac{S_1}{S_2} = \frac{C_{H1}(0,t)*C_{C2}(0,t)}{C_{H2}(0,t)*C_{C1}(0,t)} e^{-2\alpha f[(E^0_{2,HER}-E^0_{2,CO2})-(E^0_{1,HER}-E^0_{1,CO2})]} \quad \text{Equation 1a}$$

$$\frac{S_1}{S_2} = \frac{R_1}{R_2} e^{-2\alpha f[(E^0_{2,HER}-E^0_{2,CO2})-(E^0_{1,HER}-E^0_{1,CO2})]} \quad \text{Equation 1b}$$

$$\frac{S_1}{S_2} = e^{-2\alpha f[(E^0_{2,HER}-E^0_{2,CO2})-(E^0_{1,HER}-E^0_{1,CO2})]} \quad \text{Equation 2}$$

The dramatic differences in HER selectivity on 2-MPA-Au and 4-PEM-Au at lower potentials (with approximately same onset potential differences) suggest the surface concentration ratio R ($R=C_H/C_C$) must be different. Recent studies on the role of cations by Bell et al. have suggested proton donation from the dissociation of hydrated cations buffers the local electrolyte once the pKa of hydrated cations is lower than local pH.[29] Similar behavior was also observed by Kenis et al.'s study on the effect of hydrated cations on the current density of CO evolution.[30] The pKa of the functional groups are summarized in Table 2. Thus, the higher $R_{(MPA)}$ may be attributed to the lower pKa of surface ligand. The HER selectivity at higher potentials may also be attributed to the dominant surface species. As shown in the following section, the deprotonated MPA is the main species on MPA-Au (shown in the stability analysis with IR spectrum). Here, the lower pKa makes MPA both a good proton donor and poor acceptor, thus the surface concentration ratio of H^+ to CO_2 is lower at high potential. The selectivity shift from CO and

current density enhancement associated with formate evolution is further discussed in later sections.

Table 2: Summarizes the pKa of thiolate ligands

Ligands	pKa
2-Mercaptanproponic Acid, (2-MPA)	3.7[31]
4-pyridylethylmercaptan, (4-PEM)	5.2[26]
Cysteamine, (CYS)	9.25[32]

Stability Analysis

One important concern associated with the electrochemical reduction of CO_2 in the presence of functionalized surfaces is the stability of the ligand at the potentials required to reduce CO_2. Several studies have shown the cathodic desorption and dissolution of alkanethiolates on gold;[33-34] however, many thiolates are considered stable at cathodic potentials. [35] More recent *in situ* work with sum frequency generation vibrational spectroscopy by Badeli et al[27] shows that octadecanethiol ligands remain at the surface even at high cathodic potentials owing to the van der Waals interaction between alkyl chain and the low solubility in aqueous solution. Aromatic thiolates are particularly stable as the aromatic group appears to enhance surface bonding.[36] Here we carried out the ex-situ ATR-IR experiments to study the stability of ligands on Au foil.

2-Mercaptopropionic acid (MPA)

Figure 2 compares the ATR-IR spectrum between freshly prepared MPA-Au sample along with the same sample post electrolysis at -0.94V vs. RHE and post electrolysis at -1.00V vs. RHE (solution phase thiols spectra are available in the SI). In the freshly prepared electrode spectra, vibrations at 1723 cm^{-1} (a) corresponds to the C=O stretching of the COOH group. The symmetric and asymmetric stretching of the $-CH_3$ group showed up at 1372 cm^{-1} (b) and 1449 cm^{-1} (c). The C-C stretching is also observed at 1241cm^{-1} (d).[37-38] The slight shoulder at 1607 cm^{-1} (e)

and the small peak at 1421 cm^{-1} (g) correspond to the asymmetric and symmetric stretching of $-COO^-$, respectively.[38] On the spectrum of the post-electrolysis (-0.94 V vs. RHE) MPA modified Au sample, the asymmetric stretching vibration at 1583 cm^{-1} (e) with a shoulder at 1662 cm^{-1} (f) indicates the presence of the deprotonated COO^- group and COOH group, respectively. The rise of peak g coupling with peak e indicates that deprotonated ligand species dominant the surface during/after the electrolysis. The vibrations of the CH_3 group and the C-C bond remain similar in pre and post electrolysis sample. Slight shifts in wavenumbers indicate the change in configuration of the monolayer results in stronger interaction between Au surface and the functional group. However, at more negative potentials (-1.00V vs. RHE), decreased absorbance associated with $-CH_3$ group and COO- group suggests the lower concentration of surface ligand. This suggests the potential window for MPA to remain on the surface is below -0.94 V vs. RHE.

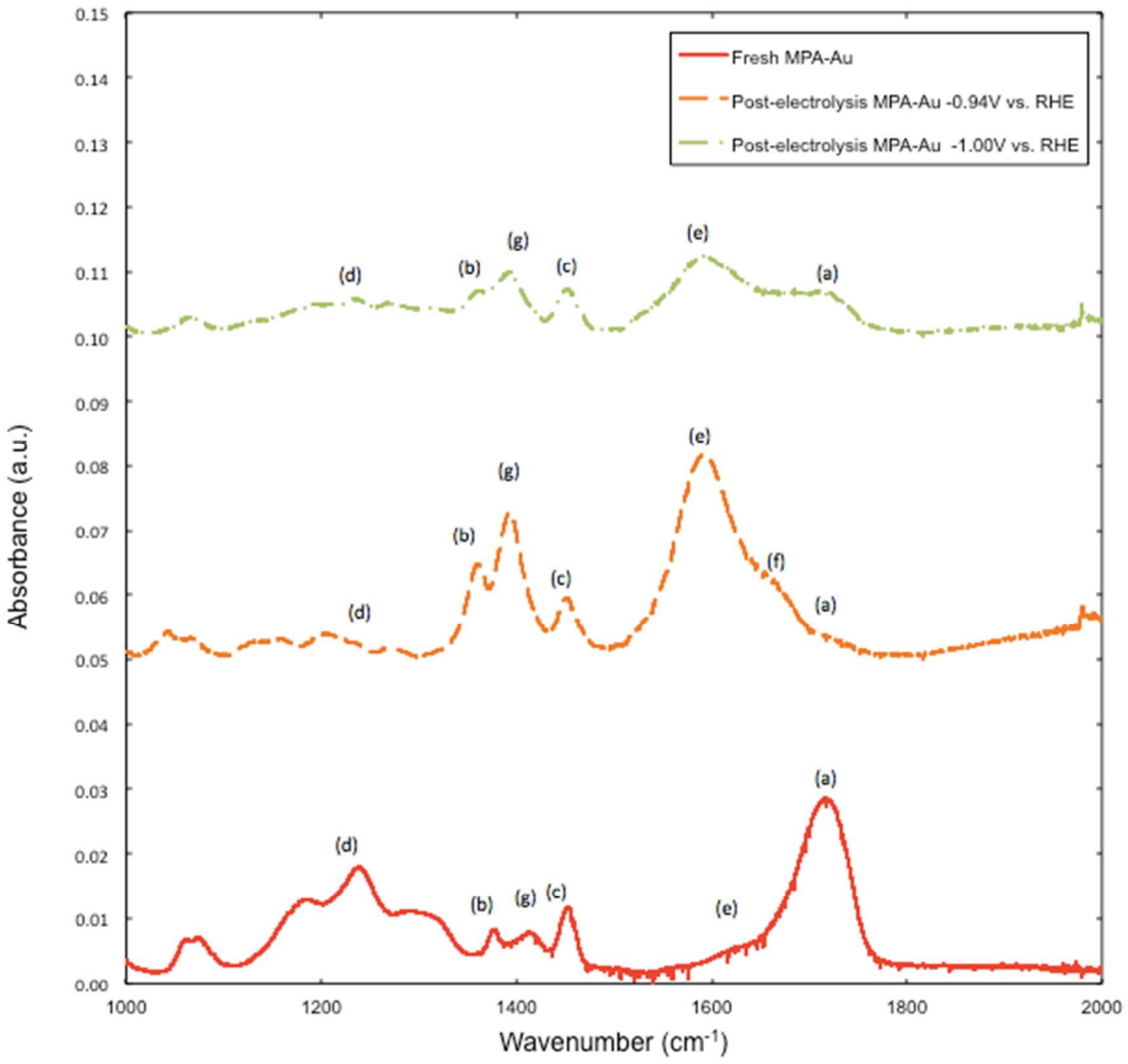

Figure 2. Comparison of ATR-IR spectra for MPA SAM on Au (a) fresh prepared (b) Post-electrolysis at -0.94V vs. RHE (c) Post-electrolysis at -1.00V vs. RHE

4-pyridylethylmercaptan (4-PEM)

Figure 3 presents the comparison between the freshly prepared 4-PEM-Au spectra and the post-reaction spectra at -1.04V vs. RHE for the sample. The bands at 1606 cm^{-1} (a), 1564 cm^{-1} (b), and 1521 cm^{-1} (c) [38-39] characterizing for the ring structures in pyridine and 780 cm-1 [(f)] and 850 cm^{-1} (e) charactering C-H deformation vibration present in both spectra. [38, 40] The vibration d was shifted from 1506 cm^{-1} to 1484 cm^{-1} indicating the presence of protonated pyridine species on the surface.[39] This indicates that the 4-pyridylethylmercaptan remains intact at -1.04 V vs.

RHE within time of electrolysis for the product analysis and further the pyridinium is the main functioning ligand in the reactions. The presence of protonated species during/after further supports the notion of ligand participation in proton transfer reactions.

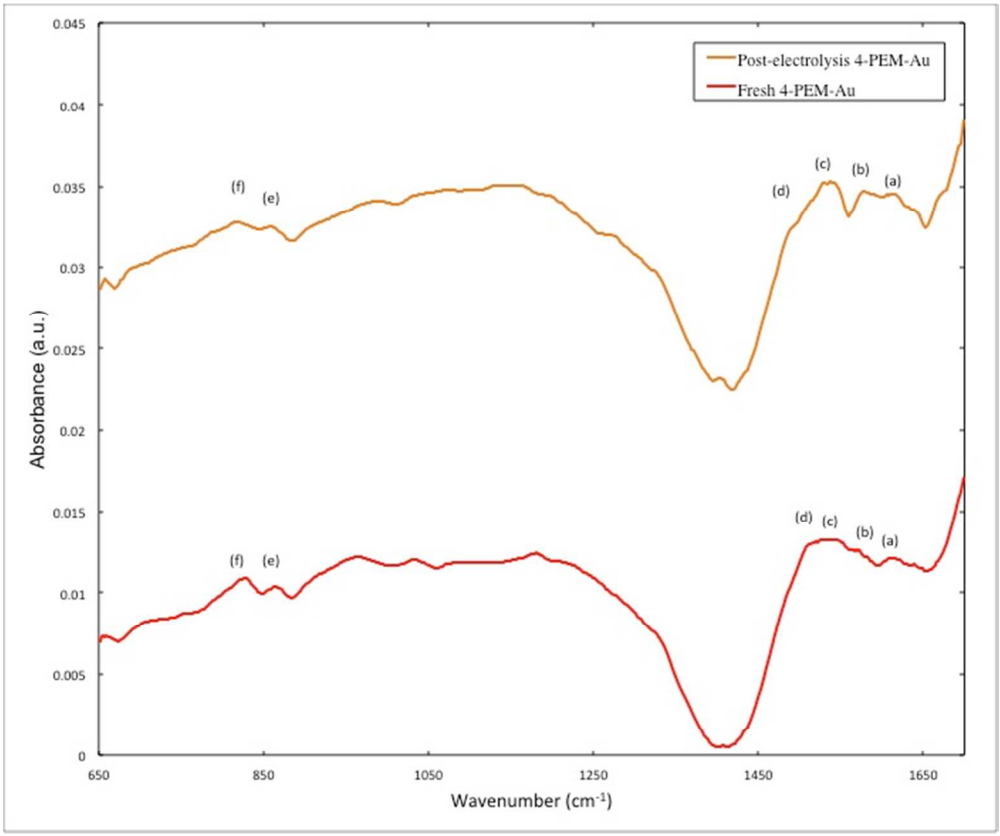

Figure 3. Comparison of ATR-IR spectra for 4-PEM SAM on Au (a) fresh prepared (b)Post-electrolysis at -1.04V vs. RHE

Cysteamine (CYS)

Figure 4 shows the comparison between the spectra of the freshly prepared CYS-Au surface and the spectra from the same electrode post electrolysis. These spectra show absorbance peaks at 1550 cm^{-1} (a), 1465 cm^{-1} (b), 1430 cm^{-1}(c), 1272 cm^{-1} (d) and 1064 cm^{-1} (e), which correspond to the N-H bonds bending vibrations, CH_2 deformation, CH_2-S wagging and C-N stretching respectively. [38, 41] Note, the solution phase ligand FTIR spectra may be found in the SI. The red shifts indicate the strong interactions between the surface and the ligand. The presence of

the absorption peaks in both spectra confirms the stability of cysteamine on the Au surfaces within the potential range of interest.

Figure 4. Comparison of ATR-IR spectra for CYS SAM on Au (a) Fresh prepared (b) Post electrolysis at -1.1V vs. RHE

Mechanism

Clearly, ligand modification of Au electrodes influences product selectivity of the CO_2 reduction reaction. Based on these results, the nature of the shifted selectivity likely originates from the separation of proton and electron transfer reactions enabled by the ligand. For example, consider the directed proton transfer behavior of enzymes involved in coupled electron transfer (PCET) reactions.[42-44] Nocera et al. showed enzymes are capable of disentangling proton transfer and electron transfer and allowing transfer coordinates on highly different length scales. In fact several studies have explored the potential of "wiring" enzymes to combine the selectivity of the natural catalysts with the advantages of externally-driven cells.[45 46 47] While there are limitations

related to the wiring of enzymes and stability concerns; there are a number of works showing functionalized electrodes, such as those considered here, are stable in the potential range needed for electrochemical reduction reactions.[18, 48-49] Given the wonderful selectivity of natural catalysts, it is likely that similar directed proton transfer reactions are possible at ligand functionalized electrodes, especially at moderate potentials.

The 3-fold increase observed in formate production when Au electrodes are functionalized with 4-PEM is remarkable. Given the presence of pyridine functional group, previous results on pyridine/Pt systems may provide some mechanistic insights. Bocarsly et al. reported the production of CH_3OH (11~39% Faradaic efficiency) and HCOOH (7~16% Faradaic efficiency) with Pt/Pd electrodes in the presence of 10mM pyridine and its substituted derivatives in the supporting electrolyte.[23, 26] Pt was reported as HER dominant (~95% Faradaic efficiency) electrocatalysts, and Pd mainly yields CO formation.[12] While the current density with the 10 mM pyridine-dosed electrolysis was relatively low (50 $\mu A/cm^2$) compared to this work (0.2~15 mA/cm^2); pyridine appears to have a strong influence in the CO_2 reduction selectivity. However, the nature specifically whether a surface or solution phase pyridinium is involved is not well established.

Initial work by Bocarsly et al. analyzed the data from cyclic voltammetry and proposed a mechanism[24] that proceeds with pyrH* as cocatalyst based on Gaussian calculations: a $1e^-$ reduction of the $pyrH^+$ to pyrH* that reacts with CO_2 and forms a CO_2-pyrH radical carbamate with inner-sphere interaction, and another surface-adsorbed H atom reacted with the surface adsorbed carbamate to yield formic acid. In that mechanism, further proton shuttling to formate yields methanol. Later work considering acidity constants for $pyrH^+$ and pyrH* by Keith and Carter showed the unfavorable deprotonation step for $pyrH^*$ since its pKa was calculated as ~27[50]. Instead, they proposed a surface mechanism[51-52] using first-principles quantum chemistry where the surface bound dihydropyridine (DHP) is the co-catalyst that takes hydride from Pt and transfers the hydride and proton to the CO_2 to yield formate.

In another study of the functional role of $pyrH^+$ during aqueous CO_2 electrochemical reduction, Batista et al. proposed an alternate proton–coupled hydride transfer mechanism[53]. The 1 e^- reduction of $pyrH^+$ produced hydride on Pt surface. CO_2 is susceptible to a 1 e^- reduction by the surface hydride coupled with another proton from $pyrH^+$. In our work, the structure of the tethered 4-PEM likely prohibits formation of DHP since the carbon atom para to N is fully bonded and does not undergo hydrogenation. Also, the thiol-tether and electron transfer requirements[54] makes the pyridinium radical formation unlikely since the electron transfer rate constant decays exponentially with the increase in donor-acceptor distance (Au and N). The electron transfer limitations also apply to Batista's proton-coupled electron transfer model where the surface hydride is replenished by the reduction of $pyrH^+$.

Here, we propose a modified formate production mechanism (depicted in Scheme 1) on 4-PEM modified Au electrodes. The first proton from aqueous solution is reduced and forms H atom adsorbed on Au (step 1a). Note the moderate pKa suggesting that the surface is not dominated by protons from the $pyrH^+$. A two-electron transfer to hyride is not plausible since the hydride dominated surface would result in HER assuming sufficient protons are available from solution. The electrophilic attack of CO_2 to the adsorbed H yields HCO_2* (step 2).[55]

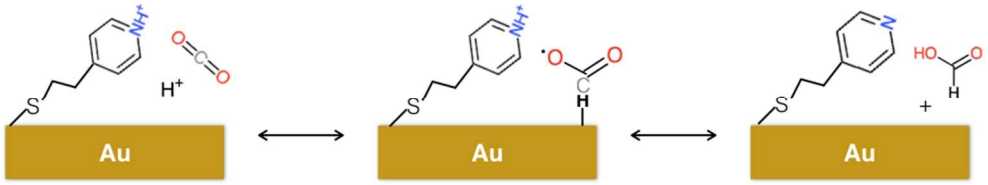

Scheme 1: Proposed Formate formation mechanism at 4-pyridylethylmercaptan modified Au surface

Compared with Au foil, the slightly higher surface concentration of H^+ (5.2 for 4-PEM versus 6.8 in 0.1M $KHCO_3$) decreases the probability of first electron transfer to CO_2^- and forms the -COOH with the proton from the solution which is the expected path to the CO evolution[6, 55-57]. Thus, a HCO_2* intermediate after the first pair of proton-electron transfer steps is likely a key

step toward the production of formate. Previous simulation studies by Norskov et al. have shown strong correlations between HCO_2* and $HCOO^-$.[55] Thus a slight selectivity shift between CO and formate is probable. Next, the tethered $pyrH^+$ in thiolate group, transfers a proton to the nearby oxygen of the HCO_2* coupled with 1e- transfer from surface (Step 3a). The enhanced HER observed at lower potentials also supports this proton-induced desorption mechanism (Step 3b). The protonated pyrH+ is replenished with proton source from the electrolyte (Step 1b).

Step 1a:

Step 1b:

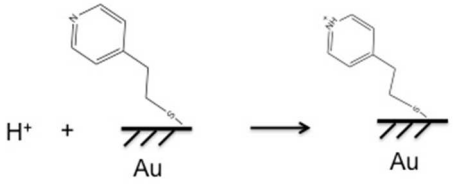

Step 2:

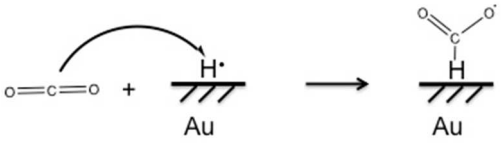

Step 3a:

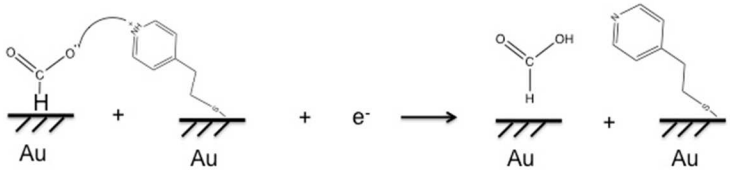

Step 3b:

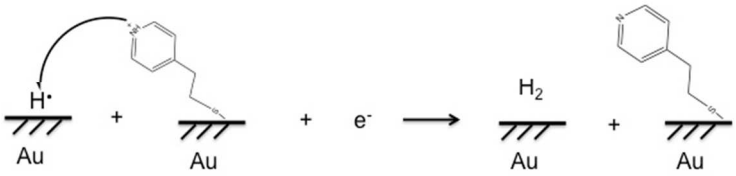

According to this mechanism, we propose that the proton donating ability (pKa) of the ligand correlates with CO_2 reduction to formate and H_2 yields as observed on functionalized Au electrodes. Ligands with low pKa values such as 2-MPA, facile proton donation favors the HER through step 3b. Ligands with high pKa, such as CYS result in diminished deprotonation as well as step 3b. Thus the product selectivity is virtually unchanged relative to untreated Au electrodes. The 2-fold enhancement in partial current density observed with CYS is likely the result of the amine's ability[58] to complex CO_2 near the surface. The intermediate pKa of 4-PEM (=5.2) facilitates the proton transfer to CO_2 in a way that yields formate.

CONCLUSION

Au electrodes functionalized with monolayers of thiol-tethered ligands were evaluated for their ability alter the selectively of CO_2 reduction reaction. A two-fold increase in Faradaic efficiency and three-fold increase in formate yield were observed with the 4-PEM-modified Au compared to the best results with untreated Au. MPA-modified Au electrodes favored only the HER and CYS-modified Au resulted in increased CO and H_2 production with virtually no changes in selectivity. A proton-induced desorption mechanism is proposed to account for the remarkable increase in formate production on 4-PEM-modified Au electrodes. The inability of the CYS and MPA-modified electrodes to yield significant amounts of formate is believed to be associated with the pKa of the surface tethered functional group. At a more fundamental level, this ligand-mediated proton transfer step demonstrates the potential for improved selectivity via "directed hydrogenation" reactions.

EXPERIMENTAL

Electrode preparation

Au foil electrodes (99.99%, ESPI) were rinsed with deionized water (MegaPure system) and used as working electrode. The functionalized electrodes were prepared as follows: Au metal foils were rinsed in deionized (DI) water followed by the solvent of ligands copiously before immersion into the 20mM of 2-mercaptopropionic acid (Sigma-Aldrich, 95%) ethanolic (Pharmco-Aaper, ACS) solution, 20mM of cysteamine (Sigma-Aldrich 95%) aqueous solution and 20mM of 4-pyridylethylmercaptan (Aldrich^{CPR}) methanolic (EMD^{TM}, ACS) solution for 10min, 10min and 5 min, respectively. Previous studies have shown short immersion times are sufficient for the chemical adsorption of thiolate at μM thiol solution to reach a packing density at $4.47*10^{-10}$ mol/cm^2.[59-60] The formation of thiol layer takes less time at higher concentration solution.[61] A well ordered pyridinylthiol monolayer on Au was studied after 5 min immersion.[40, 62] The thiolate-modified electrodes were then rinsed with solvent of the solution followed by DI water to remove the non-chemisorbed thiol and solvent molecule. A fresh electrode was prepared at each potential to ensure the consistency of the experiments.

Electrochemical Methods

Electrochemical experiments were carried out using a H-type electrochemical cell separated by Nafion membrane (FuelCellsEtc) which is to prevent the CO_2 reduction product from being reoxidized. The (functionalized) Au foil served as the cathode, while the Pt wire served as the auxiliary electrode. The potential was measured with respect to an Ag/AgCl (saturated with 3M NaCl) reference electrode (BASi, RE-5B) by a PAR model 263A potentiostat/galvanostat followed by the manual correction of uncompensated resistance. The potentials in this study were reported versus RHE with the conversion E(vs. RHE)= E(vs. Ag/AgCl)+0.197+0.059*pH. The current density was obtained by normalized with the Au geometric surface area.

Cyclic voltammetry (CV) was performed with the scanning rate at 10mV/s from 0.2V to -2.0V vs. Ag/AgCl in 0.1M $KHCO_3$ (Sigma-Aldrich, ACS reagent) as supporting electrolyte. The solution was bubbled with N_2 (Air Liquide, UHP) for 30min to produce a purged solution of pH 9 for HER reaction studies. For the CO_2 (Air Liquide, 99.99%) reduction reaction, it was purged with N_2 for 20 minutes to remove O_2, and then CO_2 was bubbled into the solution for 30 minutes producing a saturated solution with pH 6.8. The onset potentials for HER and CO_2 RR were determined from Tafel plots of CVs in N_2 saturated electrolyte and CO_2 saturated electrolyte, respectively.[63 64] (See example in SI).

For the gaseous product analyses, CO_2 was bubbled continuously into the electrochemical cell at a flow rate of 40 ml/min and a pressure of 1 atm, while potentials were applied by stepping to desired potential and held for 15 min. At the 15 min interval, the gas products (CO and H_2) in the effluent from the electrolysis were auto-sampled to the gas chromatograph (SHIMADZU, GC 2014) that equipped with FID and TCD detectors. The concentrations of individual gases were analyzed to give the production rate (expressed in partial current density, j_i) and Faradaic selectivity.

The liquid products analyses on the 30 min bulk electrolysis electrolyte were carried out with an VNMS 700 spectrometer with an excitation sculpting pulse technique for water suppression as described by Jaramillo et al.[8] 10mM DMSO was used as the reference peak. The 1D ^{1}H NMR data were processed with MestReNova. Considering the alcoholic thiol solution used here may result in false reading in higher hydrocarbon product, formate is the only liquid product discussed here.

Surface Self-Assembled Monolayer (SAM) Characterization

ATR-IR infrared spectra were measured on a smart-ITR diamond assembled Nicolet 6700 FTIR spectrometer with a nitrogen-cooled narrow-band MCT detector. Spectra were recorded for the fresh prepared electrode before any electro-reduction. The same chronoampermetry experiments for NMR electrolysis were then performed in the same two-

compartment electrochemical cell at various controlled potentials till -1.1V vs. RHE where the highest overpotential applied for the product analysis. Spectra were taken after each potential step. Interferograms were recorded at a resolution of 0.5 cm^{-1} and 256 scans. Comparison with previous reported literature excluded the possibility that the absorption peaks are from the potassium bicarbonate. [65]

ASSOCIATED CONTENT

The supporting information is available free of charge on the on the ACS Publications website.

AUTHOR INFORMATION

Corresponding Author

*johnflake@lsu.edu

ACKNOWLEDGEMENT

This work was supported by the U.S. National Science Foundation under Grant #CBET-1438385. The authors would like to thank Dr. Thomas Weldeghiorghis in the LSU Chemistry Department for his help with the NMR analysis.

REFERENCES

1. Jhong, H.-R. M.; Ma, S.; Kenis, P. J. A., Electrochemical conversion of CO2 to useful chemicals: current status, remaining challenges, and future opportunities. *Curr. Opin. Chem. Eng.* **2013,** *2* (2), 191-199.
2. Hori, Y.; Murata, A.; Takahashi, R., Formation of hydrocarbons in the electrochemical reduction of carbon dioxide at a copper electrode in aqueous solution. *J. Chem. Soc., Faraday Trans. 1* **1989,** *85* (8), 2309-2326.
3. Hori, Y.; Kikuchi, K.; Suzuki, S., PRODUCTION OF CO AND CH₄ IN ELECTROCHEMICAL REDUCTION OF CO₂ AT METAL ELECTRODES IN AQUEOUS HYDROGENCARBONATE SOLUTION. *Chem. Lett.* **1985,** *14* (11), 1695-1698.
4. Hori, Y.; Murata, A.; Takahashi, R.; Suzuki, S., Electrochemical Reduction of Carbon Monoxide to Hydrocarbons at Various Metal Electrodes in Aqueous Solution. *Chem. Lett.* **1987,** *16* (8), 1665-1668.
5. Kauffman, D. R.; Alfonso, D.; Matranga, C.; Qian, H.; Jin, R., Experimental and Computational Investigation of Au_{25} Clusters and CO_2: A Unique Interaction and Enhanced Electrocatalytic Activity. *J. Am. Chem. Soc.* **2012,** *134*, 10237-10243.
6. Zhu, W.; Michalsky, R.; Metin, Ö.; Lv, H.; Guo, S.; Wright, C. J.; Sun, X.; Peterson, A. A.; Sun, S., Monodisperse Au Nanoparticles for Selective Electrocatalytic Reduction of CO2 to CO. *J. Am. Chem. Soc.* **2013,** *135* (45), 16833-16836.
7. Yoshio Hori, A. M., Katsuhei Kikuchi, and Shin Suzuki, ElectrochemicalReduction of Carbon Dioxide to Carbon Monoxide at a Gold Electrode in Aqueous Potassium Hydrogen Carbonate. *J. Chem. Soc., Chem. Commun.* **1987**, 728-729.

8. Kuhl, K. P.; Cave, E. R.; Abram, D. N.; Jaramillo, T. F., New insights into the electrochemical reduction of carbon dioxide on metallic copper surfaces. *Energy Environ. Sci.* **2012,** *5* (5), 7050-7059.
9. Anawati; Frankel, G. S.; Agarwal, A.; Sridhar, N., Degradation and deactivation of Sn catalyst used for CO2 reduction as function of overpotential. *Electrochim. Acta* **2014,** *133*, 188-196.
10. Vesselli, E.; Rizzi, M.; De Rogatis, L.; Ding, X.; Baraldi, A.; Comelli, G.; Savio, L.; Vattuone, L.; Rocca, M.; Fornasiero, P.; Baldereschi, A.; Peressi, M., Hydrogen-Assisted Transformation of CO2 on Nickel: The Role of Formate and Carbon Monoxide. *J. Phys. Chem. Lett.* **2010,** *1* (1), 402-406.
11. Holladay, J.; Bozell, J.; White, J.; Johnson, D., Top value-added chemicals from biomass. *DOE Report PNNL* **2007,** *16983*.
12. Hori, Y., Electrochemical CO2 Reduction on Metal Electrodes. In *Modern Aspects of Electrochemistry*, Vayenas, C.; White, R.; Gamboa-Aldeco, M., Eds. Springer New York: 2008; Vol. 42, pp 89-189.
13. Shi, C.; Hansen, H. A.; Lausche, A. C.; Norskov, J. K., Trends in electrochemical CO2 reduction activity for open and close-packed metal surfaces. *Phys. Chem. Chem. Phys.* **2014,** *16* (10), 4720-4727.
14. Manthiram, K.; Beberwyck, B. J.; Alivisatos, A. P., Enhanced Electrochemical Methanation of Carbon Dioxide with a Dispersible Nanoscale Copper Catalyst. *J. Am. Chem. Soc.* **2014,** *136* (38), 13319-13325.
15. Bligaard, T.; Nørskov, J. K., Ligand effects in heterogeneous catalysis and electrochemistry. *Electrochim. Acta* **2007,** *52* (18), 5512-5516.
16. Christophe, J.; Doneux, T.; Buess-Herman, C., Electroreduction of Carbon Dioxide on Copper-Based Electrodes: Activity of Copper Single Crystals and Copper–Gold Alloys. *Electrocatalysis* **2012,** *3* (2), 139-146.
17. Watanabe, M.; Shibata, M.; Kato, A.; Azuma, M.; Sakata, T., Design of Alloy Electrocatalysts for CO 2 Reduction: III . The Selective and Reversible Reduction of on Cu Alloy Electrodes. *J. Electrochem. Soc.* **1991,** *138* (11), 3382-3389.
18. Xie, M.; Xia, B. Y.; Li, Y.; Yan, Y.; Yang, Y.; Sun, Q.; Chan, S. H.; Fisher, A. C.; Wang, X., Amino Acid Modified Copper Electrodes for the Enhanced Selective Electroreduction of Carbon Dioxide towards Hydrocarbons. *Energy Environ. Sci.* **2016,** *9* (5), 1687-1695.
19. Ogura, K.; Fujita, M., Electrocatalytic reduction of carbon dioxide to methanol. *J. Mol. Catal.* **1987,** *41* (3), 303-311.
20. Rakowski Dubois, M.; Dubois, D. L., Development of Molecular Electrocatalysts for CO2 Reduction and H2 Production/Oxidation. *Acc. Chem. Res.* **2009,** *42* (12), 1974-1982.
21. Jeoung, J.-H.; Dobbek, H., Carbon Dioxide Activation at the Ni,Fe-Cluster of Anaerobic Carbon Monoxide Dehydrogenase. *Science* **2007,** *318* (5855), 1461-1464.
22. Xiang, D.; Magana, D.; Dyer, R. B., CO2 Reduction Catalyzed by Mercaptopteridine on Glassy Carbon. *J. Am. Chem. Soc.* **2014,** *136* (40), 14007-14010.
23. Seshadri, G.; Lin, C.; Bocarsly, A. B., A new homogeneous electrocatalyst for the reduction of carbon dioxide to methanol at low overpotential. *J. Electroanal. Chem.* **1994,** *372* (1–2), 145-150.
24. Barton Cole, E.; Lakkaraju, P. S.; Rampulla, D. M.; Morris, A. J.; Abelev, E.; Bocarsly, A. B., Using a One-Electron Shuttle for the Multielectron Reduction of CO2 to Methanol: Kinetic, Mechanistic, and Structural Insights. *J. Am. Chem. Soc.* **2010,** *132* (33), 11539-11551.
25. Morris, A. J.; McGibbon, R. T.; Bocarsly, A. B., Electrocatalytic Carbon Dioxide Activation: The Rate-Determining Step of Pyridinium-Catalyzed CO2 Reduction. *ChemSusChem* **2011,** *4* (2), 191-196.

26. Barton Cole, E.; Baruch, M.; L'Esperance, R.; Kelly, M.; Lakkaraju, P.; Zeitler, E.; Bocarsly, A., Substituent Effects in the Pyridinium Catalyzed Reduction of CO2 to Methanol: Further Mechanistic Insights. *Top. Catal.* **2015,** *58* (1), 15-22.
27. Jacob, J. D. C.; Lee, T. R.; Baldelli, S., In Situ Vibrational Study of the Reductive Desorption of Alkanethiol Monolayers on Gold by Sum Frequency Generation Spectroscopy. *The Journal of Physical Chemistry C* **2014,** *118* (50), 29126-29134.
28. Bard, A. J.; Faulkner, L. R.; Leddy, J.; Zoski, C. G., *Electrochemical methods: fundamentals and applications*. Wiley New York: 1980; Vol. 2.
29. Singh, M. R.; Kwon, Y.; Lum, Y.; Ager, J. W.; Bell, A. T., Hydrolysis of Electrolyte Cations Enhances the Electrochemical Reduction of CO2 over Ag and Cu. *J. Am. Chem. Soc.* **2016,** *138* (39), 13006-13012.
30. Thorson, M. R.; Siil, K. I.; Kenis, P. J. A., Effect of Cations on the Electrochemical Conversion of CO2 to CO. *J. Electrochem. Soc.* **2013,** *160* (1), F69-F74.
31. Cannan, R. K.; Knight, B. C. J. G., Dissociation Constants of Cystine, Cysteine, Thioglycollic Acid and α-Thiolactic Acid. *Biochem. J* **1927,** *21* (6), 1384-1390.
32. Pure, I. U. o.; Data, A. C. C. o. E.; Serjeant, E. P.; Dempsey, B.; Pure, I. U. o.; Data, A. C. C. o. E., *Ionisation constants of organic acids in aqueous solution*. Pergamon Press: 1979.
33. Widrig, C. A.; Chung, C.; Porter, M. D., The electrochemical desorption of n-alkanethiol monolayers from polycrystalline Au and Ag electrodes. *Journal of Electroanalytical Chemistry and Interfacial Electrochemistry* **1991,** *310* (1–2), 335-359.
34. Byloos, M.; Al-Maznai, H.; Morin, M., Phase Transitions of Alkanethiol Self-Assembled Monolayers at an Electrified Gold Surface. *The Journal of Physical Chemistry B* **2001,** *105* (25), 5900-5905.
35. Muglali, M. I.; Erbe, A.; Chen, Y.; Barth, C.; Koelsch, P.; Rohwerder, M., Modulation of electrochemical hydrogen evolution rate by araliphatic thiol monolayers on gold. *Electrochim. Acta* **2013,** *90*, 10.1016/j.electacta.2012.11.116.
36. Srisombat, L.; Jamison, A. C.; Lee, T. R., Stability: A key issue for self-assembled monolayers on gold as thin-film coatings and nanoparticle protectants. *Colloids and Surfaces A: Physicochemical and Engineering Aspects* **2011,** *390* (1–3), 1-19.
37. Wang, Q.; Li, N., Direct Electrochemistry of Cytochrome c at a Thiolactic Acid Self-Assembled Gold Electrode. *Electroanalysis* **2001,** *13* (16), 1375-1377.
38. Socrates, G., *Infrared and Raman characteristic group frequencies: tables and charts*. John Wiley & Sons: 2004.
39. Swoboda, A.; Kunze, G., Infrared study of pyridine adsorbed on montmorillonite surfaces. *Clays Clay Miner.* **1966**, 277-88.
40. Liu, J., *Self-assembled Monolayers of Functional Group-terminated Molecules on Au*. 2010.
41. Yang, W.-h.; Li, W.-w.; Dou, H.-j.; Sun, K., Hydrothermal synthesis for high-quality CdTe quantum dots capped by cysteamine. *Mater. Lett.* **2008,** *62* (17–18), 2564-2566.
42. Cukier, R. I.; Nocera, D. G., PROTON-COUPLED ELECTRON TRANSFER. *Annu. Rev. Phys. Chem.* **1998,** *49* (1), 337-369.
43. Weinberg, D. R.; Gagliardi, C. J.; Hull, J. F.; Murphy, C. F.; Kent, C. A.; Westlake, B. C.; Paul, A.; Ess, D. H.; McCafferty, D. G.; Meyer, T. J., Proton-Coupled Electron Transfer. *Chem. Rev.* **2012,** *112* (7), 4016-4093.
44. Reece, S. Y.; Hodgkiss, J. M.; Stubbe, J.; Nocera, D. G., Proton-coupled electron transfer: the mechanistic underpinning for radical transport and catalysis in biology. *Philosophical Transactions of the Royal Society B: Biological Sciences* **2006,** *361* (1472), 1351-1364.
45. Xiao, Y.; Patolsky, F.; Katz, E.; Hainfeld, J. F.; Willner, I., " Plugging into enzymes": Nanowiring of redox enzymes by a gold nanoparticle. *Science* **2003,** *299* (5614), 1877-1881.

46. Mano, N.; Fernandez, J. L.; Kim, Y.; Shin, W.; Bard, A. J.; Heller, A., Oxygen Is Electroreduced to Water on a "Wired" Enzyme Electrode at a Lesser Overpotential than on Platinum. *J. Am. Chem. Soc.* **2003,** *125* (50), 15290-15291.
47. Heller, A., Electrical connection of enzyme redox centers to electrodes. *The Journal of Physical Chemistry* **1992,** *96* (9), 3579-3587.
48. Sirés, I.; Delucchi, M.; Panizza, M.; Ricotti, R.; Cerisola, G., Electrochemical study of self-assembled cysteine monolayers on polycrystalline gold electrodes and functionalization with microperoxidase MP-11. *J. Appl. Electrochem.* **2009,** *39* (11), 2275.
49. Fernández, J. L.; Mano, N.; Heller, A.; Bard, A. J., Optimization Of "Wired" Enzyme O2-Electroreduction Catalyst Compositions by Scanning Electrochemical Microscopy. *Angew. Chem. Int. Ed.* **2004,** *43* (46), 6355-6357.
50. Keith, J. A.; Carter, E. A., Theoretical Insights into Pyridinium-Based Photoelectrocatalytic Reduction of CO2. *J. Am. Chem. Soc.* **2012,** *134* (18), 7580-7583.
51. Keith, J. A.; Carter, E. A., Electrochemical reactivities of pyridinium in solution: consequences for CO2 reduction mechanisms. *Chemical Science* **2013,** *4* (4), 1490-1496.
52. Keith, J. A.; Carter, E. A., Theoretical Insights into Electrochemical CO2 Reduction Mechanisms Catalyzed by Surface-Bound Nitrogen Heterocycles. *J. Phys. Chem. Lett.* **2013,** *4* (23), 4058-4063.
53. Ertem, M. Z.; Konezny, S. J.; Araujo, C. M.; Batista, V. S., Functional role of pyridinium during aqueous electrochemical reduction of CO2 on Pt (111). *J. Phys. Chem. Lett.* **2013,** *4* (5), 745-748.
54. Li, T. T. T.; Weaver, M. J., Intramolecular electron transfer at metal surfaces. 4. Dependence of tunneling probability upon donor-acceptor separation distance. *J. Am. Chem. Soc.* **1984,** *106* (20), 6107-6108.
55. Feaster, J. In *Understanding Selectivity of Carbon Dioxide Reduction to Carbon Monoxide and Formic Acid on Sn Electrodes*, PRiME 2016/230th ECS Meeting (October 2-7, 2016), Ecs: 2016.
56. Zhu, W.; Zhang, Y.-J.; Zhang, H.; Lv, H.; Li, Q.; Michalsky, R.; Peterson, A. A.; Sun, S., Active and Selective Conversion of CO2 to CO on Ultrathin Au Nanowires. *J. Am. Chem. Soc.* **2014,** *136* (46), 16132-16135.
57. Chen, Y.; Li, C. W.; Kanan, M. W., Aqueous CO2 Reduction at Very Low Overpotential on Oxide-Derived Au Nanoparticles. *J. Am. Chem. Soc.* **2012,** *134* (49), 19969-19972.
58. Vaidhyanathan, R.; Iremonger, S. S.; Shimizu, G. K. H.; Boyd, P. G.; Alavi, S.; Woo, T. K., Direct Observation and Quantification of CO2 Binding Within an Amine-Functionalized Nanoporous Solid. *Science* **2010,** *330* (6004), 650-653.
59. Rouhana, L. L.; Moussallem, M. D.; Schlenoff, J. B., Adsorption of Short-Chain Thiols and Disulfides onto Gold under Defined Mass Transport Conditions: Coverage, Kinetics, and Mechanism. *J. Am. Chem. Soc.* **2011,** *133* (40), 16080-16091.
60. Buck, M.; Grunze, M.; Eisert, F.; Fischer, J.; Träger, F., Adsorption kinetics of n‐alkyl thiols on gold studied by second harmonic generation and x‐ray photoelectron spectroscopy. *Journal of Vacuum Science & Technology A* **1992,** *10* (4), 926-929.
61. Martínez, L.; Carrascosa, L. G.; Huttel, Y.; Lechuga, L. M.; Román, E., Influence of the linker type on the Au–S binding properties of thiol and disulfide-modified DNA self-assembly on polycrystalline gold. *Phys. Chem. Chem. Phys.* **2010,** *12* (13), 3301-3308.
62. Manolova, M.; Ivanova, V.; Kolb, D. M.; Boyen, H. G.; Ziemann, P.; Büttner, M.; Romanyuk, A.; Oelhafen, P., Metal deposition onto thiol-covered gold: Platinum on a 4-mercaptopyridine SAM. *Surf. Sci.* **2005,** *590* (2–3), 146-153.
63. Kim, S. K.; Zhang, Y.-J.; Bergstrom, H.; Michalsky, R.; Peterson, A., Understanding the Low-Overpotential Production of CH4 from CO2 on Mo2C Catalysts. *ACS Catalysis* **2016,** *6* (3), 2003-2013.

64. Yan, Y.; Ge, X.; Liu, Z.; Wang, J.-Y.; Lee, J.-M.; Wang, X., Facile synthesis of low crystalline MoS2 nanosheet-coated CNTs for enhanced hydrogen evolution reaction. *Nanoscale* **2013,** *5* (17), 7768-7771.
65. MILLER, F. A.; WILKINS, C. H., Infrared Spectra and Characteristic Frequencies of Inorganic Ions. *Anal. Chem.* **1952,** *24* (8), 1253-1294.

For Table of Contents only